Mechanism And Simulation Analysis Of Dynamic Balancing Of A Hollow Shaft Based On Machining Datum-Axis Correction

Guiquan Zhong, Xiaolin Yu*, and Hui Han

School of Mechanical Engineering, Shenyang Ligong University, Shenyang, Liaoning, China

Corresponding author. E-mail: flyfish513@163.com

Received: Jun. 26, 2026; Accepted: Jul. 19, 2026

To reduce unbalance in thin-walled hollow shafts without local material removal, a dynamic balancing method based on machining datum-axis correction is proposed. The method adjusts the left- and right-end machining datums during outer cylindrical finishing, causing the generated outer cylindrical axis to translate and tilt relative to the original datum axis. The existing machining allowance is thus redistributed continuously in the circumferential and axial directions, producing an equivalent compensating unbalance through the shifted centroid of the removed layer. The geometric relationship among datum correction, sectional correction vectors, and depth-of-cut variation is established. A compensation model for static and couple unbalances is derived for a constant-diameter shaft and extended to a stepped hollow shaft by considering the contributions of segment radius, length, and axial position. A Timoshenko-beam finite element model is then used to evaluate the effects of correction magnitude and direction angle on residual unbalance and synchronous vibration. The results show that correction magnitude mainly controls compensation amplitude, whereas direction angle determines compensation orientation. For the selected correction combination, continuous increased and decreased depth-of-cut regions are formed on the outer surface. At 10,000 r/min, the left and right synchronous vibration amplitudes decrease by 77.50% and 75.52%, respectively; reductions are also observed at 15,000 and 20,000 r/min.

Keywords: hollow shaft; dynamic balancing; machining datum axis; residual unbalance; synchronous vibration

http://dx.doi.org/10.6180/jase.202611_34.008

1. Introduction

With the development of drive motors for new energy vehicles toward higher rotational speed, higher power density, and lightweight design, motor rotor systems have become increasingly sensitive to initial unbalance [1, 2]. Hollow shafts, which have the advantages of low mass, small rotational inertia, and high material utilization, have been widely used in high-speed rotor structures. However, during blank forming, heat treatment, inner-hole machining, outer cylindrical finishing, and assembly positioning, factors such as wall-thickness deviation, material inhomogeneity, clamping error, and heat-treatment deformation may cause the sectional centroid of a hollow shaft to deviate from the designed rotational axis, leading to a non-uniformly distributed mass eccentricity along the axial direction [3]. During high-speed rotation, this mass eccentricity generates synchronous centrifugal excitation, which further increases the dynamic bearing reaction, enhances rotor whirl, and amplifies the vibration of the support system [4, 5]. Conventional rotor dynamic balancing usually reduces unbalance by adding or removing mass on discrete correction planes [6]. However, for high-speed thin-walled hollow shafts, local drilling, milling, or grinding may change the continuity of the outer cylindrical surface, the local wall thickness, and the sectional geometry. Therefore, achieving high-precision dynamic balancing correction while maintaining the geometric continuity and structural integrity of hollow shafts remains a key issue in the manufacturing and operational reliability control of high-speed motor shafts.

Existing studies on the unbalance dynamics of hollow shafts and rotor systems have mainly focused on unbalance response modeling, parameter identification, and dynamic balancing correction. Al-Falahat established a finite element model of a composite hollow-shaft system, investigated the effects of unbalance and rotational speed on the vibration response of hollow shafts, and further analyzed the improvement of hollow-shaft unbalance response through compensating masses [7, 8]. With the development of model-driven dynamic balancing methods, unbalance parameters can be identified using steady-state or transient vibration responses, thereby reducing the number of trial weights and start-stop operations to some extent [4, 5, 9–11, 21–23]. Nevertheless, at the implementation level, these methods still mainly rely on adding or removing mass on discrete correction planes. To avoid the influence of conventional material removal on structural integrity, active balancing techniques have been applied to adjust the compensating mass distribution in real time during rotor operation. Pan et al. proposed a liquid transfer active balancing system for high-speed hollow rotors, in which compensating mass is generated by liquid transfer between oppositely arranged chambers to reduce unbalance vibration [12]. Fieux et al. proposed an internal bending actuator for rotors, which changes the bending state of the rotor through an internal actuation mechanism to compensate for inherent eccentricity caused by manufacturing errors and to suppress synchronous vibration [13]. However, active balancing methods usually require additional sensors, actuators, control units, or internal transmission structures, which may increase the structural complexity of the system and impose higher requirements on real-time control and reliability under high-speed operating conditions.

In addition to active compensation during operation, the influence of manufacturing and machining processes on the actual geometric state and dynamic response of rotating components has also attracted increasing attention. Shekhar et al. analyzed the combined effects of clamping error, tool geometric error, spindle error motion, and unbalance excitation on the actual radial trajectory of a high-speed spindle [14]. Liu et al. proposed a virtual-machining-based optimization method for the machining centerline of crankshafts, in which the mass distribution and dynamic balancing state of the machined crankshaft were improved by searching for the machining centerline position [15]. These studies indicate that the machining datum not only affects the geometric accuracy of shaft components, but also changes the final mass distribution and dynamic balancing state by altering the material removal position [14, 15]. Recent studies on intelligent engineering systems also show that geometry-aware state estimation, spatiotemporal registration, and objective-driven trajectory optimization can improve spatial perception and motion planning in complex robotic scenarios [24–27]. However, for thin-walled hollow shafts, an explicit analytical model is still lacking for reducing both static unbalance and couple unbalance through the adjustment of the left and right machining datums without forming local material-removal regions.

Based on the above analysis, this paper proposes a dynamic balancing method for hollow shafts based on machining datum-axis correction. The proposed method is intended for the outer cylindrical finishing stage of hollow shafts. In this method, the residual machining allowance is used as a continuously adjustable material-removal source. By adjusting the positions of the left and right machining datums, the generated outer cylindrical axis is controllably corrected relative to the original machining datum axis, thereby changing the distribution of local depth of cut in both the circumferential and axial directions. Unlike conventional local material removal, the proposed method changes the centroid position of the removed layer during final finishing, so that the remaining shaft body obtains an equivalent compensating unbalance opposite to the initial unbalance. Based on this idea, the geometric relationship between machining datum-axis correction and local depth-of-cut redistribution is first established, and the influence of corrected machining on the centroid of the removed layer and the equivalent compensating unbalance is analyzed. Then, the analytical relationship between datum correction and static unbalance as well as couple unbalance is derived for a uniform-diameter hollow shaft and further extended to a stepped hollow shaft composed of multiple uniform-diameter shaft sections. Finally, based on a Timoshenko beam model, the variations in residual unbalance and synchronous vibration response before and after datum correction are analyzed.

2. Methods

2.1. Depth-of-Cut Variation Induced by Datum-Axis Correction

The unbalance state of a machined hollow shaft is affected by the initial mass distribution, wall-thickness deviation, clamping and positioning errors, and the position of outer-cylinder material removal [3]. In this study, the correction quantity is not generated by local removal or additional weights. Instead, the left- and right-end machining datums are adjusted during outer cylindrical finishing so that the removed layer is redistributed and the existing machining allowance forms an equivalent compensating unbalance.

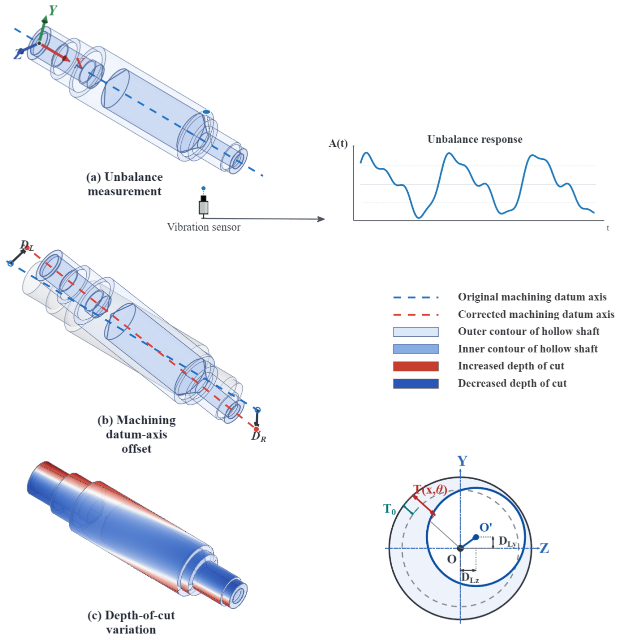

Fig. 1. Dynamic balancing principle of a hollow shaft based on machining datum-axis correction

The basic procedure is shown in Fig. 1. Fig. 1(a) shows the initial unbalance measurement process. Fig. 1(b) shows the datum-axis correction, where the blue dashed line denotes the original machining datum axis and the red dashed line denotes the corrected machining datum axis. Fig. 1(c) shows the resulting depth-of-cut redistribution. The red and blue regions indicate increased and decreased depth of cut relative to the theoretical uniform depth of cut under the original datum condition, respectively.

According to Fig. 1, let the shaft axial direction be x, and let y and z be the two radial directions in the cross-section. Taking the original machining datum axis as the reference axis, the left- and right-end datum correction vectors are denoted by $\mathbf{D}_L$ and $\mathbf{D}_R$. Under the small-correction condition, the correction at an arbitrary axial position is obtained by linear interpolation between the two end corrections; the circumferential variation in depth of cut and the corresponding compensation of static and couple unbalances can then be established.

A fixed coordinate system $O-XYZ$ is established, where the rotating axis of the hollow shaft is the X-axis and Y and Z denote the two orthogonal directions in the cross-section. Let the original machining datum axis be the X-axis, the axial coordinate be x, the shaft length be L, the outer radius be R_f, and the initial radial depth of cut be T_0. In this study, the left- and right-end machining datum correction vectors are used as control variables to determine the spatial position of the generated outer cylindrical axis. The datum-axis correction vector is defined as

$$\mathbf{D}_L = \left[D_{Ly}, D_{Lz}\right]^{\mathrm{T}}, \quad \mathbf{D}_R = \left[D_{Ry}, D_{Rz}\right]^{\mathrm{T}} \tag{1}$$

where D_{Ly} and D_{Lz} are the corrections of the left-end datum in the y,z direction, and D_{Ry} and D_{Rz} are the corrections of the right-end datum in the y,z direction. At an arbitrary axial position x, the transverse correction of the corrected machining datum axis relative to the original datum axis is given by

$$\mathbf{s}(x) = \left(1 - \frac{x}{L}\right)\mathbf{D}_L + \frac{x}{L}\mathbf{D}_R \tag{2}$$

where $s(x)$ denotes the transverse correction vector of the corrected machining datum axis relative to the original machining datum axis X at axial position x, and its magnitude represents the distance between the two axes in that section. The left- and right-end datum corrections jointly determine the generated outer cylindrical axis after finishing. When the two end corrections are identical, the datum axis mainly undergoes rigid translation; when they differ, the datum axis is tilted. Let the circumferential angle of the outer cylinder be θ; the actual radial depth of cut can then be expressed as

$$T(x,\theta) = T_0 - \mathbf{s}^{\mathrm{T}}(x)\begin{bmatrix}\cos\theta \\ \sin\theta\end{bmatrix} \tag{3}$$

Eq. (3) indicates that datum correction introduces a first-order harmonic depth-of-cut component on the basis of the theoretical radial depth of cut. The y-direction corrections determine the cosine component, whereas the z-direction corrections determine the sine component. Under the small-correction assumption, the removed volume after datum correction can be approximated as

$$\Delta V = \int_0^{2\pi}\int_0^{L} R_f T(x,\theta)\,\mathrm{d}x\,\mathrm{d}\theta \tag{4}$$

Because the circumferential integrals of the sine and cosine terms over $0 \sim 2\pi$ are zero, the first-order approximation keeps the total removed volume unchanged. Datum correction therefore mainly redistributes the removed material in the circumferential and axial directions, producing a controlled centroid offset of the removed layer and providing the geometrical basis for equivalent compensating unbalance.

2.2. Analytical Relationship Between Datum Correction and Unbalance

During operation, mass eccentricity produces synchronous centrifugal excitation and can be described by resultant static and couple unbalance vectors [4, 6, 7, 21–27]. In this study, the continuously removed mass induced by datum correction is treated as an equivalent compensating mass field. Let the magnitude and phase of the initial static unbalance be U_s, ϕ_s, those of the couple unbalance be U_m, ϕ_m, and the material density be ρ. Taking the axial midpoint $x = L/2$ as the reference point, the static unbalance compensation generated by the removed mass is

$$\Delta \mathbf{U}_s = \frac{\rho\pi\left(R_f - T_0\right)^2 L}{2}\left(\mathbf{D}_L + \mathbf{D}_R\right) \tag{5}$$

The couple unbalance compensation generated by the removed mass is

$$\Delta \mathbf{U}_m = \frac{\rho\pi\left(R_f - T_0\right)^2 L^2}{12}\left(\mathbf{D}_L - \mathbf{D}_R\right) \tag{6}$$

Eq. (5) and Eq. (6) show that the average component of the two end corrections mainly affects static unbalance, whereas their differential component mainly affects couple unbalance. Therefore, the four correction components can be jointly adjusted to construct the target machining datum axis. Under ideal conditions, the initial unbalance is counteracted by the compensation generated through datum correction, namely

$$\begin{aligned} U_s \begin{bmatrix}\cos\phi_s \\ \sin\phi_s\end{bmatrix} + \frac{\rho\pi\left(R_f - T_0\right)^2 L}{2}\left(\mathbf{D}_L + \mathbf{D}_R\right) &= \mathbf{0} \\ U_m \begin{bmatrix}\cos\phi_m \\ \sin\phi_m\end{bmatrix} + \frac{\rho\pi\left(R_f - T_0\right)^2 L^2}{12}\left(\mathbf{D}_L - \mathbf{D}_R\right) &= \mathbf{0} \end{aligned} \tag{7}$$

The left- and right-end datum corrections are then obtained as

$$\begin{aligned} \mathbf{D}_L &= -\frac{U_s}{\rho\pi\left(R_f - T_0\right)^2 L}\begin{bmatrix}\cos\phi_s \\ \sin\phi_s\end{bmatrix} + \frac{6U_m}{\rho\pi\left(R_f - T_0\right)^2 L^2}\begin{bmatrix}\cos\phi_m \\ \sin\phi_m\end{bmatrix} \\ \mathbf{D}_R &= -\frac{U_s}{\rho\pi\left(R_f - T_0\right)^2 L}\begin{bmatrix}\cos\phi_s \\ \sin\phi_s\end{bmatrix} - \frac{6U_m}{\rho\pi\left(R_f - T_0\right)^2 L^2}\begin{bmatrix}\cos\phi_m \\ \sin\phi_m\end{bmatrix} \end{aligned} \tag{8}$$

The above analytical relationship is obtained for a constant-diameter outer cylinder. In practice, hollow shafts usually have an obvious stepped configuration, and the final radius and axial length differ among shaft segments. To preserve the analytical form of the model, the stepped hollow shaft is represented as a combination of n constant-diameter shaft segments. The axial range of the ith segment is $x \in [x_{i-1}, x_i]$, its segment length is L_i, and its final outer radius is denoted by $R_{f,i}$. Each segment satisfies the compensation mechanism of a constant-diameter segment within its local range; therefore, the stepped-shaft model can be obtained by accumulating the geometrical contributions of all shaft segments.

$$\begin{aligned} \mathbf{D}_L &= -\frac{U_s}{\rho\pi}\sum_{i=1}^{n}\frac{1}{\left(R_{f,i} - T_0\right)^2 L_i}\begin{bmatrix}\cos\phi_s \\ \sin\phi_s\end{bmatrix} + \frac{6U_m}{\rho\pi}\sum_{i=1}^{n}\frac{1}{\left(R_{f,i} - T_0\right)^2 L_i^2}\begin{bmatrix}\cos\phi_m \\ \sin\phi_m\end{bmatrix} \\ \mathbf{D}_R &= -\frac{U_s}{\rho\pi}\sum_{i=1}^{n}\frac{1}{\left(R_{f,i} - T_0\right)^2 L_i}\begin{bmatrix}\cos\phi_s \\ \sin\phi_s\end{bmatrix} - \frac{6U_m}{\rho\pi}\sum_{i=1}^{n}\frac{1}{\left(R_{f,i} - T_0\right)^2 L_i^2}\begin{bmatrix}\cos\phi_m \\ \sin\phi_m\end{bmatrix} \end{aligned} \tag{9}$$

In Eq. (9), the first summation group corresponds to static-unbalance compensation, and the second group corresponds to couple-unbalance compensation. The contribution of each shaft segment is jointly determined by its outer radius, axial length and axial position, so the stepped outer geometry directly affects the required datum correction.

3. Results and discussion

3.1. Simulation Object and Modeling Parameters

A stepped hollow-shaft rotor for an electric-drive motor is used as the simulation object. Its axial profile, inner-hole structure, and support positions are shown in Fig. 2. To describe the axial variations in mass and bending stiffness, the shaft is discretized using Timoshenko beam elements [16–19]. The total length is 242.2 mm, and the shaft is divided into 14 beam elements and 15 nodes. The left and right supports are applied at node 2 ($x = 5.0$ mm) and node 14 ($x = 237.6$ mm), respectively.

Because different shaft segments have different radii and inner-hole dimensions, the sectional area, second moment of area, and mass per unit length are calculated segment by segment [16–20]. Table 1 lists the main parameters used for finite element modeling and unbalance response calculation.

The initial unbalance state is determined from the amplitudes and phases on the left and right measurement planes

[21–27]. In the representative case, the static unbalance is $U_s = 9.80\ \mathrm{g \cdot mm}$ with $\phi_s = 9.37°$, and the couple unbalance is $U_m = 419.10\ \mathrm{g \cdot mm^2}$ with $\phi_m = 191.72°$. This state is used for datum-correction solution and vibration response calculation.

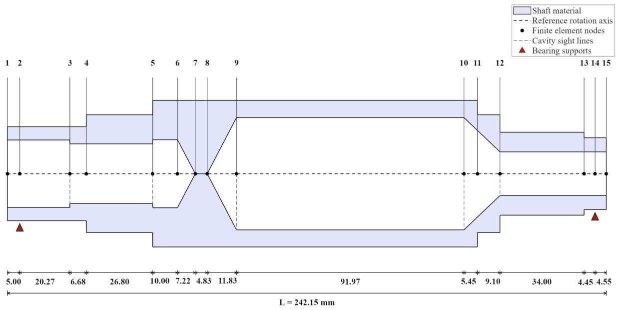

Fig. 2. Geometry and finite element discretization of the stepped hollow shaft

Table 1. Parameters of the hollow shaft.

Parameter	Symbol	Value
Total length of the hollow shaft	L	242.15 mm
Density	ρ	$7.85 \times 10^3\ \mathrm{kg/m^3}$
Elastic modulus	E	210 GPa
Bearing stiffness	k	$1 \times 10^8\ \mathrm{N/m}$
Bearing damping	c	500 N·s/m
Poisson's ratio	ν	0.30
Depth of cut	T_0	0.20 mm
Total mass of the hollow shaft	M	1.74 kg

3.2. Effects of Datum Correction Parameters on Residual Unbalance

Datum correction is a two-dimensional vector described by correction magnitude and direction angle: $D_L = |D_L| \angle \phi_L$ and $D_R = |D_R| \angle \phi_R$. The magnitudes mainly control the centroid offset of the removed layer, whereas the direction angles determine the circumferential positions of the increased- and decreased-depth-of-cut regions. To identify the parameter effects, the left- and right-end magnitudes are first swept under a prescribed direction relationship, and the residual static unbalance $|U_{s,r}|$ and residual couple unbalance $|U_{m,r}|$ are calculated. Fig. 3 shows that increasing the correction magnitude initially enhances compensation, but excessive correction may lead to overcompensation and local rebound of the residual unbalance.

The nonmonotonic trend in Fig. 3 is caused by the transition from insufficient compensation to overcompensation. When the correction magnitude is small, depth-of-cut redistribution is weak and the equivalent compensating unbalance is insufficient to offset the initial unbalance. As the magnitude increases, the centroid offset of the removed layer increases and the compensating unbalance approaches the required value, reducing both residual static and couple unbalances. If the magnitude continues to increase, the compensating unbalance may exceed the required amount, and the residual unbalance rises again. The different minimum points also indicate that the left and right datum corrections contribute differently to static and couple unbalances.

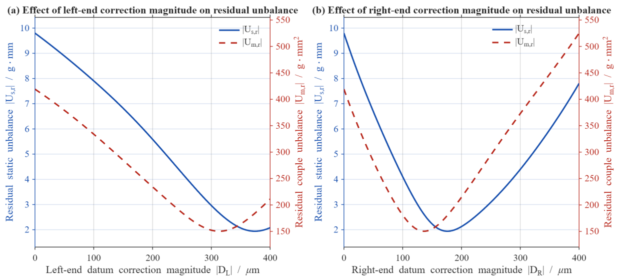

Fig. 3. Effects of datum correction magnitude on residual static unbalance and residual couple unbalance

The left- and right-end datum corrections simultaneously change the rigid translation and axial tilt of the generated outer cylindrical axis. For the same magnitude, different direction angles change the circumferential positions of the increased- and decreased-depth-of-cut regions, thereby changing the centroid-offset direction and residual-unbalance phase. Therefore, both magnitude and direction angle must be considered. Fig. 4 shows the effects of the left- and right-end direction angles on residual static and couple unbalances under representative correction magnitudes.

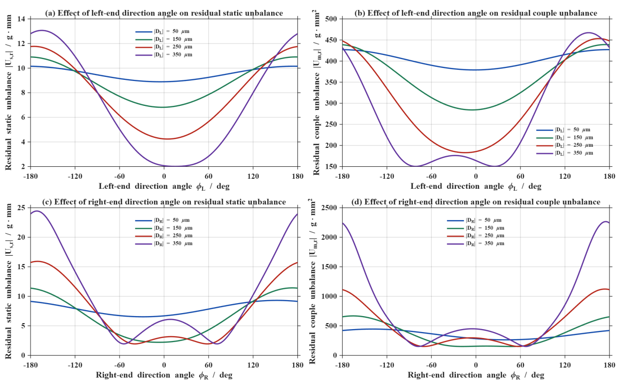

Fig. 4. Effects of left- and right-end direction angles on residual unbalance under different datum correction magnitudes

As shown in Fig. 4, residual unbalance varies periodically and nonmonotonically with direction angle. A suitable angle makes the compensating unbalance better match the initial unbalance, whereas an unsuitable angle increases the residual component. The sensitivity to direction angle also increases with correction magnitude because a larger centroid offset amplifies angular error. Since Fig. 3 and Fig. 4 show that low-residual regions of static and couple unbalances do not fully coincide, a final correction combination cannot be selected from a single end parameter or a single residual component.

To clarify the selection basis, the left and right datum correction parameters were determined by jointly considering the residual static and couple unbalances. During the parameter search, a combination was not selected if it reduced only one component while clearly increasing the other. The preferred combination was the one that kept both residual components at relatively low levels within the allowable correction range. According to this coordinated-reduction criterion, the combination marked in Fig. 5 was selected as the final correction combination.

Based on this criterion, the left- and right-end magnitudes and direction angles are scanned separately while the opposite-end parameters remain at the current low-residual combination. Fig. 5 shows the resulting residual-unbalance distributions, where the horizontal coordinate is correction magnitude, the vertical coordinate is direction angle, and the color represents residual unbalance. The star marker denotes the selected combination: $|\mathbf{D}_L| = 317.135\ \mu\text{m}$, $\phi_L = 6.612°$, $|\mathbf{D}_R| = 145.193\ \mu\text{m}$, and $\phi_R = -2.812°$.

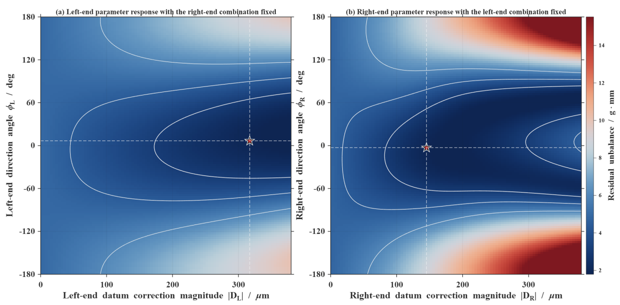

Fig. 5. Effects of datum correction magnitude and direction angle on residual unbalance under joint correction conditions

3.3. Characteristics of Depth-of-Cut Distribution After Datum Correction

Fig. 6 shows the spatial distribution of depth-of-cut variation under the selected correction combination. The red and blue regions indicate increased and decreased depth of cut relative to the original datum condition, respectively. The variation is distributed continuously over the outer surface rather than being confined to a local correction plane, and the increased- and decreased-depth regions vary along the axial direction, confirming that the corrected datum axis contains both rigid translation and axial tilt.

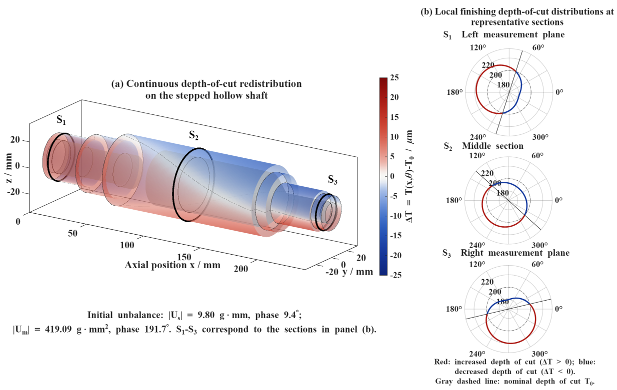

Fig. 6. Spatial distribution of depth-of-cut variation and typical sections under the selected datum correction combination

In Fig. 6(b), the distributions at S_1, S_2, and S_3 have different magnitudes and phases. The left and right measurement planes are mainly affected by the corresponding end corrections, while the middle section reflects the transition between them. Thus, the continuously varying centroid offset can regulate both static and couple unbalances instead of providing only local compensation.

3.4. Synchronous Vibration Response Before and After Datum Correction

The balancing effect is finally evaluated by the reduction in synchronous vibration response at the measurement points [6, 9–11, 21–27]. The unbalances before and after datum correction are applied as synchronous centrifugal excitations in the Timoshenko-beam finite element model, and the responses at nodes 2 and 14 are extracted. Table 2 compares the response amplitudes at different speeds, and Fig. 7 shows the corresponding vibration orbits.

Table 2 and Fig. 7 show that datum correction reduces the synchronous vibration responses at both measurement points. At 10,000 r/min, the left and right amplitudes decrease from 4.336 and 4.388 μm to 0.976 and 1.074 μm, corresponding to reductions of 77.50% and 75.52%, respectively. Reductions are also obtained at 15,000 and 20,000 r/min. The vibration orbits shrink after correction, indicating effective suppression of transverse synchronous vibration.

Table 2. Synchronous vibration amplitudes and reductions before and after datum correction at different rotational speeds.

Rotational speed / r·min^{-1}	Left measurement point before correction / μm	Left measurement point after correction / μm	Reduction at the left measurement point / %	Right measurement point before correction / μm	Right measurement point after correction / μm	Reduction at the right measurement point / %
10000	4.336	0.976	77.50	4.388	1.074	75.52
15000	1.285	0.605	51.87	1.955	0.940	51.90
20000	1.154	0.616	46.63	1.399	0.788	43.66

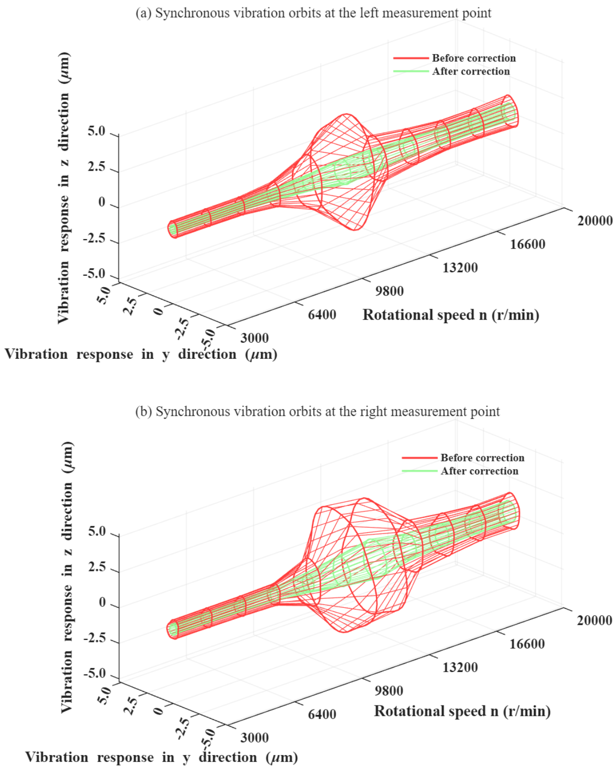

Fig. 7. Synchronous vibration orbits at the left and right measurement points before and after datum correction

4. Conclusions

This study proposes a dynamic balancing method for high-speed stepped hollow shafts based on machining datum-axis correction to address the problem that conventional local material removal may damage the surface continuity and local wall thickness of the outer cylinder. By independently adjusting the left- and right-end machining datum positions, the corrected machining datum axis undergoes controlled translation and tilt relative to the original machining datum axis. As a result, the spatial distribution of the removed layer changes in the circumferential and axial directions, and an equivalent compensating unbalance is generated to counteract the initial unbalance. The geometrical relationship among datum correction, sectional correction vectors and outer cylindrical depth-of-cut redistribution is established, and the compensation relationships for static and couple unbalances of the hollow shaft are derived. On this basis, a Timoshenko-beam finite element model is used to perform a parametric analysis of datum correction, and the effects of correction magnitude and direction angle on residual unbalance, spatial distribution of the outer cylindrical depth of cut and synchronous vibration response are investigated. The main conclusions are as follows.

(1) The geometrical relationship among the left- and right-end datum corrections, sectional correction vectors and outer cylindrical depth-of-cut redistribution is established. The rigid translation and axial tilt of the corrected machining datum axis relative to the original machining datum axis form a first-order harmonic depth-of-cut variation in the section and cause the increased- and decreased-depth-of-cut regions to evolve continuously along the axial direction. Under the first-order small-correction approximation, datum correction mainly changes the circumferential distribution of material removal without changing the total removed volume of the section.

(2) For a constant-diameter uniform hollow shaft, the average component of the left- and right-end corrections mainly controls the rigid translation of the generated outer cylindrical axis and plays a dominant role in static-unbalance compensation. The differential component mainly controls the axis tilt and plays a dominant role in couple-unbalance compensation. For a stepped hollow shaft, the compensation contribution of each shaft segment is also affected by its outer radius, axial length and position relative to the moment reference plane.

(3) The parametric analysis shows that the datum correction magnitude mainly determines the amplitude of the equivalent compensating unbalance, whereas the correction direction angle mainly determines the circumferential orientation of the compensation effect. As the correction magnitude increases, the residual static and couple unbalances generally first decrease and then tend to level off or rebound. The minimum positions of the two residual un-

balance components do not completely coincide. Therefore, the left- and right-end correction magnitudes and direction angles must be determined jointly, rather than being selected based only on a single end parameter or a single residual unbalance component.

(4) The Timoshenko-beam finite element results show that datum correction can effectively reduce the synchronous vibration response of the hollow shaft. At 10,000 r/min, the synchronous amplitudes at the left and right measurement points decreased from 4.336 μm and 4.388 μm to 0.976 μm and 1.074 μm, respectively, corresponding to reductions of 77.50% and 75.52%. At 15,000 and 20,000 r/min, the responses after correction are also lower than those before correction, indicating that the proposed method suppresses unbalance vibration at different rotational speeds.

The proposed method is mainly applicable to hollow shafts that still have a residual machining allowance for outer cylindrical finishing and whose left and right machining datums can be controllably adjusted before final finishing. Under these conditions, the residual machining allowance can be used as a continuously distributed material-removal source, and unbalance compensation can be achieved by changing the local depth-of-cut distribution while avoiding the influence of conventional local material removal on the surface continuity and local wall thickness of the hollow shaft.

It should also be noted that the proposed method is not applicable to finished shafts that have completed final outer cylindrical machining and have no remaining machining allowance. It is also not suitable for machining systems that cannot accurately adjust the datum axis. In practical applications, the actual correction effect may be affected by the initial machining allowance distribution, datum positioning error, clamping repeatability, machine-tool motion accuracy, and unbalance measurement error. Therefore, the datum correction magnitude should be constrained by the residual machining allowance, the allowable depth-of-cut variation, and the final dimensional accuracy requirements.

Acknowledgment

The authors gratefully acknowledge the financial support from the Liaoning Provincial Applied Basic Research Program (Grant No. 2025JH2/101300056).

References

[1] Q. Shen, Z. Zhou, S. Li, X. Liao, T. Wang, X. He, and J. Zhang, (2022) *"Design and Analysis of the High-Speed Permanent Magnet Motors: A Review on the State of the Art"* **Machines** ***10***(7): 549. DOI: 10.3390/machines10070549.

[2] H. Zhao, J. Li, X. Zhang, B. Xiong, C. Zhao, Y. Ruan, H. Wang, J. Zhang, Z. Lan, X. Huang, and H. Zhang, (2024) *"State-of-the-Art Lightweight Implementation Methods in Electrical Machines"* **Machines** ***12***(5): 339. DOI: 10.3390/machines12050339.

[3] C. Fu, J.-J. Sinou, W. Zhu, K. Lu, and Y. Yang, (2023) *"A State-of-the-Art Review on Uncertainty Analysis of Rotor Systems"* **Mechanical Systems and Signal Processing** ***183***: 109619. DOI: 10.1016/j.ymssp.2022.109619.

[4] C.-L. Lin, J.-W. Liang, Y.-M. Huang, and S.-C. Huang, (2023) *"A Novel Model-Based Unbalance Monitoring and Prognostics for Rotor-Bearing Systems"* **Advances in Mechanical Engineering** ***15***(1): 16878132221148019. DOI: 10.1177/16878132221148019.

[5] M. A. d. C. Michalski, I. S. de Melo, and G. F. M. de Souza, (2025) *"Dynamic Unbalance Identification in Steady-State Rotating Machinery: A Hybrid Methodology Integrating Physical and Data-Driven Techniques"* **Journal of Sound and Vibration** ***597***: 118817. DOI: 10.1016/j.jsv.2024.118817.

[6] L. Li, S. Cao, J. Li, R. Nie, and L. Hou, (2021) *"Review of Rotor Balancing Methods"* **Machines** ***9***(5): 89. DOI: 10.3390/machines9050089.

[7] A. M. Al-Falahat, (2021) *"Examination of the Dynamic Behaviour of the Composite Hollow Shafts Subject to Unbalance"* **International Journal of Mechanical Engineering and Robotics Research** ***10***(10): 572–576. DOI: 10.18178/ijmerr.10.10.572-576.

[8] A. M. Al-Falahat, (2022) *"Implementation of the Dynamic Balancing Approach of a Rotating Composite Hollow Shaft"* **EUREKA: Physics and Engineering** (2): 68–73. DOI: 10.21303/2461-4262.2022.002336.

[9] S. Zhao, X. Ren, W. Deng, K. Lu, Y. Yang, and C. Fu, (2021) *"A Transient Characteristic-Based Balancing Method of Rotor System without Trail Weights"* **Mechanical Systems and Signal Processing** ***148***: 107117. DOI: 10.1016/j.ymssp.2020.107117.

[10] S. Zhao, X. Ren, W. Deng, K. Lu, Y. Yang, L. Li, and C. Fu, (2021) *"A Novel Transient Balancing Technology of the Rotor System Based on Multi Modal Analysis and Feature Points Selection"* **Journal of Sound and Vibration** ***510***: 116321. DOI: 10.1016/j.jsv.2021.116321.

[11] S. Zhao, X. Ren, Q. Zheng, K. Lu, C. Fu, and Y. Yang, (2022) *"Transient Dynamic Balancing of the Rotor System with Uncertainty"* **Mechanical Systems and Signal Processing** ***171***: 108894. DOI: 10.1016/j.ymssp.2022.108894.

[12] X. Pan, Z. Xie, J. Lu, H. Wu, J. Gao, and Z. Jiang, (2019) *"Novel Liquid Transfer Active Balancing System for Hollow Rotors of High-Speed Rotating Machinery"* **Applied Sciences *9***(5): 833. DOI: 10.3390/app9050833.

[13] G. A. Fieux, N. Y. Bailey, and P. S. Keogh, (2024) *"A Novel Rotor Internal Bend Actuator for the Wireless Compensation of Inherent Eccentricities"* **Mechanical Systems and Signal Processing *213***: 111306. DOI: 10.1016/j.ymssp.2024.111306.

[14] S. Shekhar, S. Nahata, and O. B. Ozdoganlar, (2020) *"The Effect of Spindle Dynamics on Tool-Tip Radial Throw in Micromachining"* **Journal of Manufacturing Processes *56***: 1397–1403. DOI: 10.1016/j.jmapro.2020.04.036.

[15] Z. Liu, Y. Luo, and T. W. Liao, (2024) *"Optimization of Crankshaft Machining Center-Line Based on Virtual Machining Method"* **International Journal of Automotive Engineering *15***(2): 98–105. DOI: 10.20485/jsaeijae.15.2_98.

[16] Y. Yang, Q. Wu, Y. Wang, W. Qin, and K. Lu, (2019) *"Dynamic Characteristics of Cracked Uncertain Hollow-Shaft"* **Mechanical Systems and Signal Processing *124***: 36–48. DOI: 10.1016/j.ymssp.2019.01.035.

[17] A. M. Al-Falahat, (2023) *"Analysis and Modelling of the Rotor Dynamics of a Composite Hollow Shaft Using Finite Element Techniques"* **International Journal of Advanced Technology and Engineering Exploration *10***(101): 485–497. DOI: 10.19101/IJATEE.2022.10100553.

[18] F. Stoop, S. Meier, P. Civelli, J. Mayr, and K. Wegener, (2023) *"Multi-Variable Rotor Dynamics Optimization of an Aerostatic Spindle"* **CIRP Journal of Manufacturing Science and Technology *42***: 12–23. DOI: 10.1016/j.cirpj.2023.01.006.

[19] Y. Yang, J. Wang, Y. Wang, C. Fu, Q. Zheng, and K. Lu, (2021) *"Dynamical Analysis of Hollow-Shaft Dual-Rotor System with Circular Cracks"* **Journal of Low Frequency Noise, Vibration and Active Control *40***(3): 1227–1240. DOI: 10.1177/1461348420948287.

[20] O. Ahmed, T. A. El-Sayed, and H. Sayed, (2024) *"Finite Element Analyses of Rotor/Bearing System Using Second-Order Journal Bearings Stiffness and Damping Coefficients"* **Journal of Vibration and Control *30***(17–18): 3961–3984. DOI: 10.1177/10775463231204388.

[21] T. Choudhury, R. Viitala, E. Kurvinen, R. Viitala, and J. Sopanen, (2020) *"Unbalance Estimation for a Large Flexible Rotor Using Force and Displacement Minimization"* **Machines *8***(3): 39. DOI: 10.3390/machines8030039.

[22] G. Ranjan and R. Tiwari, (2020) *"On-Site High-Speed Balancing of Flexible Rotor-Bearing System Using Virtual Trial Unbalances at Slow Run"* **International Journal of Mechanical Sciences *183***: 105786. DOI: 10.1016/j.ijmecsci.2020.105786.

[23] F. D. Sanches, A. A. J. Cavallini, and V. J. Steffen, (2024) *"Theoretical and Experimental Applications of a Rotor Balancing Technique without Using Trial Weights Based on Augmented Kalman Filter"* **Mechanical Systems and Signal Processing *208***: 111066. DOI: 10.1016/j.ymssp.2023.111066.

[24] Q. Yang, D. Li, M. Li, and L. Liu, (2026) *"A Fractional-Order Spatiotemporal Unified Energy Framework for Non-Repetitive LiDAR Point Cloud Registration"* **Fractal and Fractional *10***(1): 42. DOI: 10.3390/fractalfract10010042.

[25] Q. Yang, D. Li, X. Zhang, X. Cai, and S. Sun, (2026) *"A Composite Objective-Driven Framework for High-Performance Robotic Trajectory Optimization"* **Journal of Applied Science and Engineering *32***(26032012): 1. DOI: 10.6180/jase.202609_32.012.

[26] Q. Yang and J. Xu, (2026) *"Representation Enhancement for Geometry-Guided Monocular 6D Pose Estimation in Occluded Scenes"* **Journal of Applied Science and Engineering *33***(26033001): 1. DOI: 10.6180/jase.202610_33.001.

[27] L. Li, Z. Liu, and Q. Yang, (2026) *"Efficient 6D Pose Estimation via Lightweight Backbone and Dense Multimodal Fusion"* **Journal of Applied Science and Engineering *32***(26032002): 1. URL: https://www.researchgate.net/publication/408191572_Efficient_6D_Pose_Estimation_Via_Lightweight_Backbone_And_Dense_Multimodal_Fusion.